RSC Advances

PAPER

View Article Online
View Journal | View Issue

Cite this: *RSC Adv.*, 2024, **14**, 9038

Fabrication of zinc oxide nanorods for photocatalytic degradation of docosane, a petroleum pollutant, under solar light simulator

Ahmed K. Alsharyani[ab] and L. Muruganandam *[a]

The use of advanced oxidation processes (AOP) in photocatalysis is critical for treating hazardous chemical compounds in oil-produced water (OPW). ZnO NRs are one of the most important modern and safe photocatalysts and have been easily prepared by a microwave-assisted hydrothermal method and grown on glass substrates. Hexagonal-shaped ZnO NRs and a bandgap energy (E_g) of up to 3.2 eV were characterized using SEM, XRD, UV-Vis, and PL devices, respectively. The effectiveness of photocatalytic degradation on the organic docosane solution was evaluated using a solar light simulator. On the surface area of the ZnO NRs, high photon absorption causes e^-/h^+ pairs to be excited between the VB and CB, producing free radicals that immediately react with organic contaminants and transform them into harmless chemicals. The photocatalytic degradation efficiency of the compound docosane analysed using GC-MS/MS reached 68.5% at 5 hours of irradiation. A mechanism for the photocatalytic degradation of docosane was proposed at pH ~ 6.5, and a reduction of 60.5% of the total organic carbon (TOC) was achieved. Thus, the photocatalytic treatment of organic compounds contained in OPW has great potential and serves an important environmental purpose.

Received 26th January 2024
Accepted 28th February 2024

DOI: 10.1039/d4ra00672k

rsc.li/rsc-advances

1. Introduction

The production of crude oil and natural gas is one of the most important sources of wealth, and energy demand is on the rise, but environmental and economic repercussions and obstacles are encountered during the extraction of this energy, resulting in the production of enormous quantities of oil-produced water OPW.[1] OPW is a byproduct of the injection of pure water into onshore and offshore wells and subsequent extraction of crude oil and natural gas.[2,3] The quantity of OPW produced contributes significantly to the volume of waste generated by oil and gas extraction due to the presence of hazardous substances. Global crude oil production is approximately 80 million barrels per day, whereas OPW production is approximately 250 million barrels per day, which raises environmental and economic concerns.[4,5] The volume ratio of the discharge of OPW is not constant and can increase or decrease based on geographical location, the age of the well, and production techniques employed.[6] The characteristics and concentrations of hazardous substances in OPW can vary depending on the condition of oil wells throughout the operation. Heavy organic hydrocarbons (aliphatic and aromatic), dissolved solids, phenols, naphthalene, and various other toxic compounds found in OPW contribute to environmental damage.[7] Organic hydrocarbon compounds are a major source of pollution in OPW and are found in complex forms and as a mix of straight-chain or branched-chain hydrocarbons.[8,9] Straight-chain hydrocarbon alkanes (*n*-alkanes) such as octadecane, hexadecane, eicosane, heneicosane, docosane, tricosane, octacosane, and similar hydrocarbon compounds with higher molecular weight in OPW make it difficult to treat. Organic compounds with low molecular weights (such as phenol and some alkanes ($<C_{10}$)) that have been completely processed are easily disposed off because they are less toxic and less water-soluble.[10,11] Any hydrocarbon compounds in OPW that constitute an environmental danger must be appropriately regulated, as their toxicity when discharged into water result in ecological and economic challenges for the restoration of this water. One hydrocarbon compound found in OPW is the organic compound docosane (*n*-docosane), a saturated aliphatic long-chain hydrocarbon ($C_{22}H_{46}$).[12] It is one of the harmful and complex compounds found in high concentrations in petroleum water and promotes water pollution.[13,14] Additionally, it has a greater molecular weight and is therefore closely related to hazardous chemical compounds that harm the marine ecosystem.[15] Because of their toxic nature (alkanes) and persistence in water with significant concentration, they pose a threat to human health (*e.g.*, mutagenesis and carcinogenesis) and ecosystems.[16,17]

Numerous methods are employed in the management and treatment of OPW for the elimination of hydrocarbons and other hazardous compounds.[18] Advanced oxidation processes (AOP),

[a]*School of Chemical Engineering, Vellore Institute of Technology University, India. E-mail: LMN@vit.ac.in*

[b]*Nanotechnology Research Center, Sultan Qaboos University, Muscat, Oman*

membrane filtration, biological treatment, treatment with additive chemicals and adsorption, and many other methods have been studied for the treatment of OPW.[19,20] Some OPW treatment approaches are inefficient at removing minerals, dissolved hydrocarbons, and additives due to the geographical location.[21,22] The optimum technology for the advanced oxidation process (AOP) would be good for the environment and cost less to run, which would make it superior to others. During the advanced treatment of OPW, it is essential to satisfy water quality standards and comprehend the treatment technology pathway in terms of understanding the characteristics of by-products and their impacts when recycled or disposed off in the ecosystem. Advanced oxidation processes (AOP) are one of the safe and effective new methods for treating OPW that can remove and destroy harmful organic molecules.[23] Photocatalysis is one of the applications of advanced oxidation processes enhanced by solar or UV irradiation to generate hydroxyl radicals ($OH^{\bullet}$) and superoxide radical ions ($^{\bullet}O_2^-$) that react with toxic organic compounds and convert them into water (H_2O), carbon dioxide (CO_2)and other by-product compounds.[24,25]

The efficient harnessing of solar irradiation energy in the wastewater treatment process supported by nanomaterials from semiconductors (as a photocatalytic degradation method) is very efficient, environmentally and economically appropriate.[26] Fe_2O_3, ZnO, TiO_2, and WO_3 are nanostructured semiconductor-based photocatalysts that are utilized in a variety of applications, including the elimination of pollutants from wastewater.[27,28] In addition, various morphologies of nanomaterials, such as nanorods, nanoflowers, nanotubes, nanoparticles, nanospheres, and nanowires, have been used for many applications including sensors and catalysts.[29,30] Based on their intended use, nanomaterials may be synthesized using various techniques, such as microwave-assisted hydrothermal, sol–gel, pulsed laser, or spray pyrolysis methods.[27]

Zinc oxide nanorods (ZnO NRs) are among the most versatile substances utilised in medicine, photocatalysis, and as anticancer and antibacterial agents due to a number of distinguishing qualities. Nanorods can develop on easily removed supports following the photocatalytic process. When ZnO nanorods are attached to a support, their surface-to-volume ratio is greater than that of other nanoparticulate films, which leads to greater adsorption of organic molecules.[31] The surface area and surface defects of metal oxide nanoparticles enhance their photocatalytic efficacy by facilitating active redox reactions that aid in the breakdown of organic molecules. In addition, ZnO is a good photocatalyst as one of the latest green environmental technologies that are readily available and cost-effective in the process of removing contaminants from water.[29,32]

So far, relatively little significant research has been reported in the literature on the photocatalytic degradation of the compound docosane in OPW-supported ZnO NRs under solar light. In this study, ZnO nanorods produced using a hydrothermal technique aided by microwaves were employed for the photocatalytic degradation of a docosane pollutant solution. Using XRD, SEM, PL, and UV-visible analysis, the characterization of the ZnO NRs produced on tiny glass substrates was studied. In addition to analytical parameters pH and total organic carbon (TOC), GC-MS/MS was utilized to explore the photocatalytic degradation process of the petroleum pollutant docosane.

2. Materials and methods

2.1. Chemicals

To fabricate the ZnO NRs on glass substrates (25 mm × 75 mm), analytical reagents such as zinc nitrate hexahydrate [$Zn(NO_3)_2 \cdot 6H_2O$; purity >99.8%] was obtained from Sigma Aldrich. Zinc acetate dihydrate ($Zn(CH_3OO)_2 \cdot 2H_2O$; purity >99% Merck) and hexamethylenetetramine ($C_6H_{12}N_4$; purity >99% Merck) were purchased from Billerica, USA. The docosane (*n*-docosane, purity >99% Sigma Aldrich) was supplied by Supelco, Bellefonte, USA, and ethanol (C_2H_6O, purity >99%, Sigma Aldrich) and deionized water were used to prepare all aqueous solutions.[24] Throughout the experiment, organic solvents with purity levels greater than analytical grade were utilised.

2.2. Synthesis of the ZnO NRs by a microwave-based hydrothermal method

A hydrothermal technique was used to fabricate the ZnO NRs on glass substrates. Dust-free glass substrates were cleaned with soap, then with ethanol and acetone, and finally with DI water (15 minutes each step) to ensure that they were free of suspended microbial sediments. These glass substrates were dried in an oven at 90 °C and later placed on a hot plate at 350 °C. In a typical synthesis, zinc acetate dihydrate was prepared and dissolved in DI water to obtain a 10 mM seed solution of ZnO. The aqueous seed solution was sprayed directly onto the glass substrates in the form of a layer. Solutions of zinc nitrate hexamine and hexamethylenetetramine were dissolved separately in DI water to obtain 20 mM of the growth solution mixture of the ZnO NRs. For the microwave-assisted hydrothermal process, the glass substrates were immersed in the growth solution, treated in a microwave at 180 W for 45 minutes, and allowed to cool for 15 min. To ensure the growth of the ZnO NRs, the process of immersing glass slides was repeated 4 times with same steps, and the growth solution was replaced with a new solution. The glass slides were washed with DI water to remove suspended and undesirable sediments and later placed in an oven to dry at 90 °C. The ZnO-NR-coated array samples were annealed in a furnace operated at 350 °C for an hour to improve the crystalline structure and photocatalytic activity of the ZnO NRs.[11,33]

2.3. ZnO NR characterization

The ZnO NRs on the glass substrates were characterized using X-ray diffraction (XRD), scanning electron microscopy (SEM), photoluminescence (PL), and UV-Vis spectroscopy. The crystal structure and orientation of the ZnO NRs were investigated using an X-ray diffractometer (Rigaku RINT 2100, XRD) operated using Cu-Kα radiation (wavelength 0.154 nm) and recorded in the 2θ angle range from 20°–80° in steps of 0.02° s^{-1}. The morphological structure of the ZnO NRs was investigated using a scanning electron microscope (JSM-7600F, JEOL) operated at 20 kV. An SEM energy dispersive spectrometer (EDS) was used to analyse the composition of the ZnO NRs. The surface defects of

the ZnO NR samples were investigated using photoluminescence spectroscopy (PerkinElmer LS55) with a 325 nm excitation wavelength. The optical absorption spectra of the ZnO NRs were determined in the wavelength range of 300–800 nm using UV-Vis spectroscopy (Lambda25, PerkinElmer).

2.4. Photocatalytic degradation activity experiment for docosane

The photocatalytic performance of the pure ZnO NRs was evaluated *via* the degradation of a 10 ppm docosane solution, prepared by dissolving docosane in ethanol and DI water. Later, 3.5 mL of the docosane solution was poured into a glass cuvette with the ZnO NR substrate (0.9 cm × 3 cm) and a control sample without the ZnO NRs. The glass cuvettes were stored for 2 h in a dark place to achieve adsorption and desorption equilibrium of the samples with ZnO NR surfaces. The glass cuvettes were then subjected to a solar light simulator (Sciencetech SSI1.6 kW) with 1.1 kW m^{-2} of irradiance.

Solar light simulators are used as an alternative to natural sunlight in various applications and scientific tests and facilitate control of the field of light and ensure the accuracy of experimental results.[24,34] The photocatalytic process was continued for 5 h, during which 0.5 mL samples were collected every hour to evaluate the concentration and other parameters of the docosane solutions using GC-MS/MS (GCMS-TQ8040, non-polar capillary column, Shimadzu, Japan) spectroscopy, a pH (S220, Seven Compact) meter and total organic content (TOC-VCSH, Shimadzu) analyser. By incorporating the

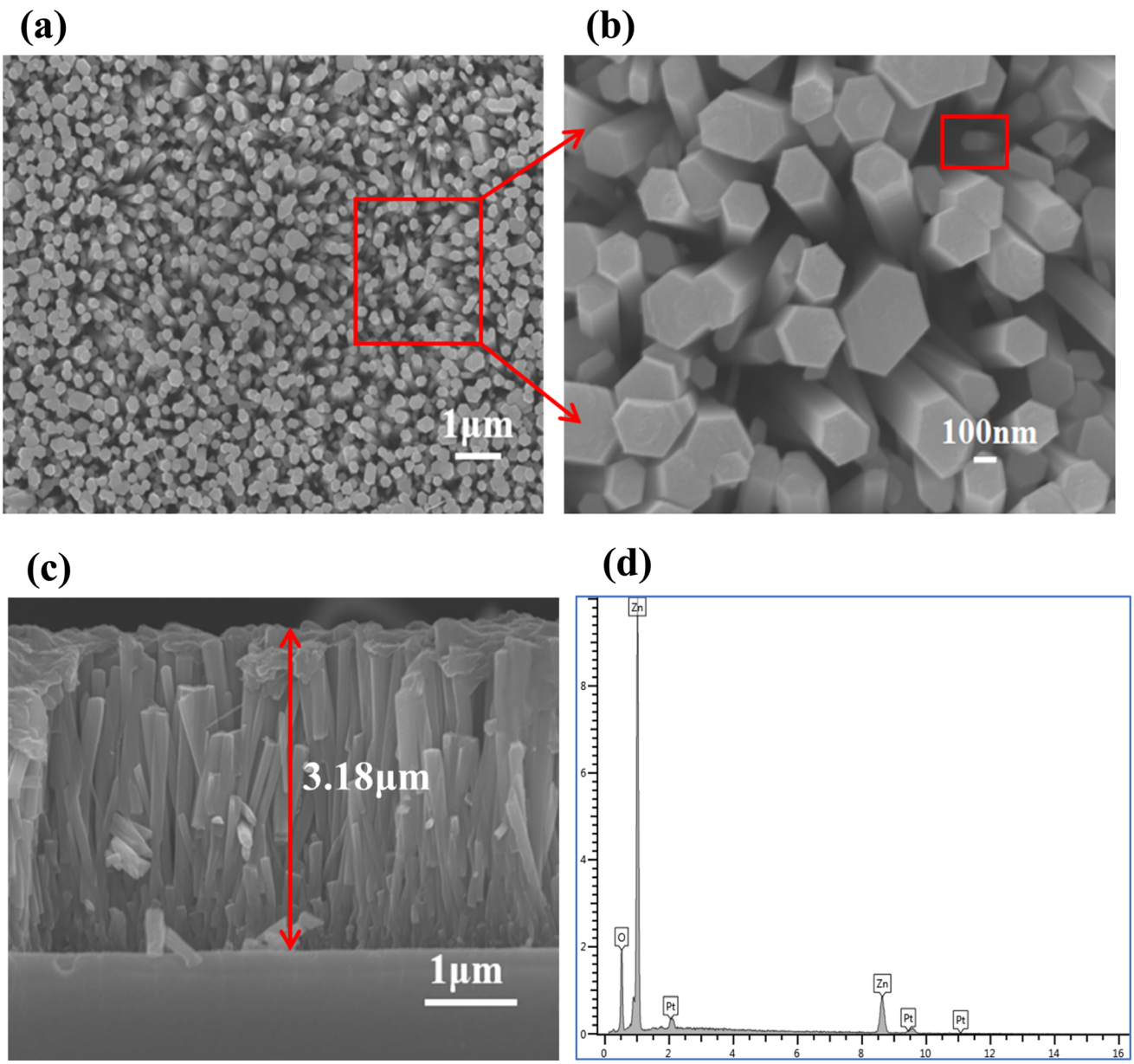

Fig. 1 SEM images of the ZnO NRs: (a) top view of the ZnO NR surface at low magnification and (b) high magnification, (c) cross-sectional view and vertical length of 3.18 μm of the ZnO NRs and (d) EDS spectrum of the elemental composition of the ZnO NRs.

reusability of ZnO NR catalysts into the photocatalytic degradation process, practical costs may be reduced, and the effectiveness of the ZnO NRs can be evaluated under controlled experimental conditions.[35]

3. Results and discussion

3.1. SEM analysis

The morphological structure properties of ZnO NRs grown on a glass substrate were studied using a scanning electron microscope (SEM), as presented in Fig. 1. The adoption of the microwave-assisted hydrothermal process method and annealing at a temperature of 350 °C during the fabrication of the ZnO NRs led to the formation of hexagonal interconnected rods. This was confirmed by the top view depicted in Fig. 1(a) and (b), as indicated in ref. 36. The cross-sectional view reveals vertically connected rods of varying sizes, as indicated in Fig. 1(c). SEM and energy dispersive spectrometry (EDS) were used to determine the composition of the ZnO NRs. Fig. 1(d) indicates the presence of peaks for elements zinc (Zn) and oxygen (O) in proportions of 79.2% and 20.8%, respectively. In addition to the sample, the element platinum (Pt) used to implant the sample in the device produces a peak.

3.2. XRD analysis

The hexagonal structural data and phase purity of the ZnO NRs as determined using XRD are illustrated in Fig. 2. The diffraction peaks of the vertically aligned ZnO NRs at different 2θ positions indicate excellent crystallinity of the structure.[37] The diffractions of the ZnO NRs were observed at 30.90°, 34.30°, 37.50°, 47.44°, 62.76°, and 72.48°, with associated planes of (100), (002), (101), (102), (103) and (004), respectively. These values were indexed to the hexagonal wurtzite ZnO NRs according to their match with the standard JCPDS card No. 01-070-8070, confirming the successful synthesis of the ZnO NRs. All observed peaks related to ZnO have distinct peak intensities, and no impurity traces were observed. The peak intensity of the ZnO NR (002) plane at $2\theta = 34.4°$ was greater compared to other phase peaks.[38] This high intensity implies that the ZnO NRs are grown in a preferred *c*-axis orientation. Using the Debye–Scherrer equation and full width at half maximum values of the diffraction peaks, the average crystallite size of the ZnO NR sample was estimated to be around 36.6 nm.[39,40]

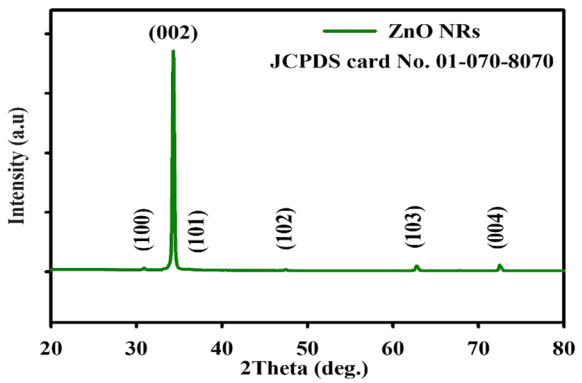

Fig. 2 XRD pattern of the synthesized ZnO NRs.

3.3. UV-Vis spectroscopy analysis

The optical properties of the ZnO NR sample in terms of absorption peaks in the wavelength range between 300 and 800 nm were determined using UV-Vis spectroscopy, as shown in Fig. 3(a). The optical analysis of the ZnO NR sample indicates the weak absorption in the visible light region and strong absorption peaks in the UV light region at wavelengths of 300–380 nm.

The highest characteristic absorption intensity of the ZnO NRs is at ~350 nm, which contributes to the enhanced generation of electrons of the sample in the photocatalytic process by absorbing photons. The optical bandgap energy (E_g) of the ZnO NR structure in the high absorption spectrum range can be calculated using the Tauc model with the following equation:[41]

$$(\alpha h\nu)^{1/2} = C(h\nu - E_g)^m, \quad (1)$$

where bandgap energy (E_g) of sample ZnO NRs is 3.2 eV, C is a constant (an inverse proportionality constant to $h\nu$), h is the Planck's constant (1240), ν is related to the frequency of the photon (nm), $m = 0.5$ is the constant of semiconductors and α is the optical absorption coefficient.[42] The absorption coefficient (α) is evaluated based on the film thickness used *via* the following relation:

$$\alpha = \frac{(2.303)A}{t}, \quad (2)$$

where A is the absorbance and t is the film thickness of the sample. As shown in Fig. 3(b), the straight line obtained from the plot of $(\alpha h\nu)^2$ on the *y*-axis *versus* photon energy ($h\nu$) on the *x*-axis, the E_g for the ZnO NR sample is around 3.2 eV at $\alpha = 0$ (34). Furthermore, optical E_g may decrease due to impurity density, which leads to a decrease in carrier concentration and increases tensile stress and oxygen vacancies, causing intrinsic defects that reduce the average crystallite size. Likewise, the quantum confinement effect occurs in thin films of ZnO, which are typically less than the size of bulk ZnO, reaching about 3.37 eV.[43,44]

3.4. Photoluminescence (PL) analysis

The PL spectra at room temperature were utilized to quantify the optical characteristics of semiconductors and to determine the recombination efficiency of photo-excited charge carriers in the sample. Thus, the PL spectrum of the pure ZnO NR sample was used to evaluate crystal defects under excitation emission at around 325 nm (~3.8 eV), as visualized in Fig. 4(a). The intensity of the PL spectra is attributable to the recombination rate efficiency of electron/hole (e^-/h^+) pair photogenerated charge carriers in the sample. Thus, a larger spectrum intensity denotes more e^- and h^+ pairs, while a lower intensity indicates fewer e^- and h^+ pairs. By analysing the PL spectra of the ZnO NRs sample, the near-band-edge UV emission at 375 nm (~3.3 eV) that contributes to the transition of the e^-/h^+ pairs from the conduction band (CB) to the valence band (VB) of the semiconductors can be identified. In addition, the emission spectra

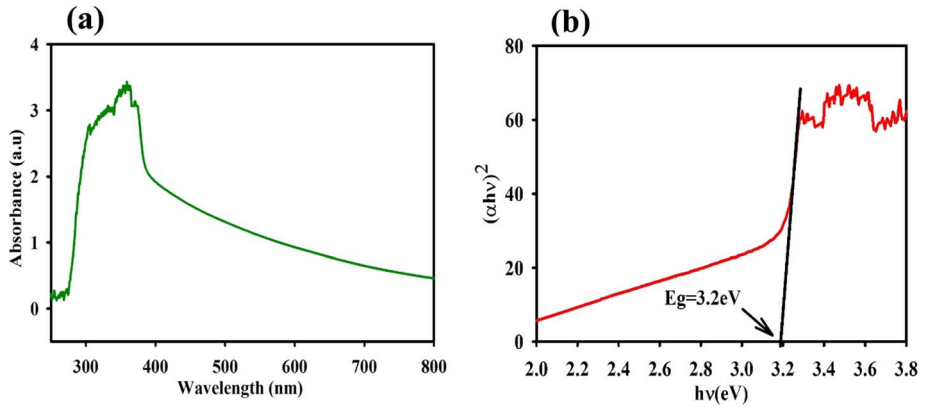

Fig. 3 (a) Typical absorption spectrum and (b) optical bandgap energy *via* Tauc model analysis of the ZnO NRs.

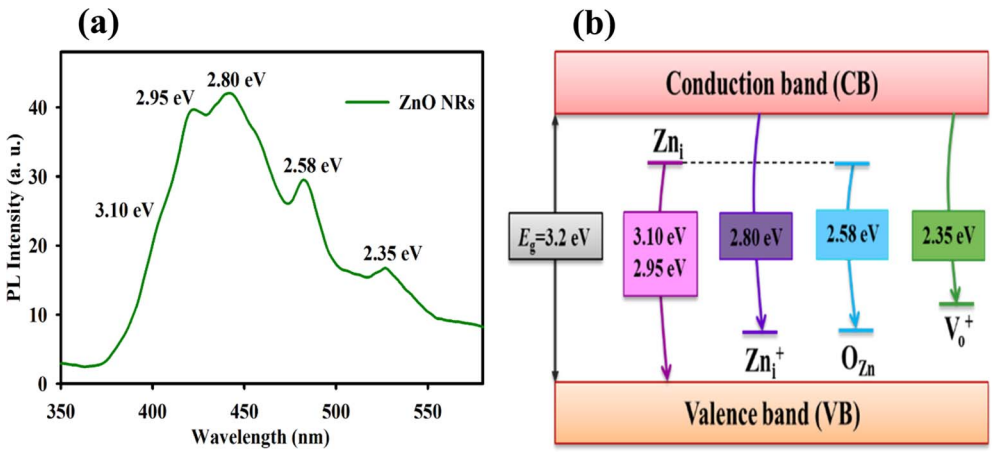

Fig. 4 (a) PL emission spectra of the ZnO NRs at room temperature. (b) Mechanism of emission bands from transitions involving energy defect states in the ZnO NRs.

of ZnO NRs display five major peaks centered at 404 nm, 420 nm, 443 nm, 480 nm, and 526 nm, which correspond to energies of 3.10 eV, 2.95 eV, 2.80 eV, 2.58 eV, and 2.35 eV, respectively, indicating that the sample exhibits superior crystal quality.[42]

In addition, emission band peaks between the UV and visible region are located in the violet (400–425 nm), indigo (425–450 nm), blue (450–480 nm), and green (485–550 nm) regions of the PL spectrum. The trapping mechanism of the e^-/h^+ pairs corresponding to the broad peaks of the crystal defects in the ZnO NR sample is often indicative of the levels of Zn vacancies (V_{Zn}), Zn interstitials (Zn_i), O vacancies (V_o), O interstitials (O_i) and O antisites (O_{Zn}) with different charges.[45]

The scheme shown in Fig. 4(b) depicts the trapping mechanisms of the band (CB and VB) energy levels of free exciton charge carriers in the defect states of the ZnO NRs. These emissions from different kinds of defects in the sample, such as violet emissions at 404 nm and 420 nm, which correspond to photon energies of 3.10 eV and 2.95 eV, respectively, have been attributed to Zn interstitials (Zn_i).[46] Hence, the defect emission level in ZnO indicates a substantial number of Zn_i defects caused by the utilization of the microwave-assisted hydrothermal method during the synthesis of the ZnO NRs.[47] The broad band of indigo emission centered at 443 nm (2.80 eV) was attributed to a Zn_i^+ charge.[48] In addition, a blue luminescence emission peak was observed at 480 nm (2.58 eV), which was assigned as antisite oxygen (O_{Zn}), due to transitions from the CB to O_{Zn} to near the VB.[24,46]

The violet-blue emission of the ZnO NR sample in the wavelength region of 400–480 nm has great application potential in light emission and bioluminescence.[49,50] The small peak located at ~526 nm (2.35 eV) corresponding to the green emission of the ZnO NRs was identified as an oxygen vacancy (V_o^+) defect.[51] The green luminescence peak observed in the deep emission level of the trap state may originate due to the transitions for the recombination of a photoexcited e^- and h^+ at an oxygen vacancy (V_o^+).[45,52] Oxygen vacancy (V_o^+) and Zn interstitials (Zn_i) are two predominant intrinsic defects that have been reported to be appropriate for photocatalysis activity. Generally, the association of e^-/h^+ pairs trapped in ZnO NR defects with surface-adsorbed O_2 and OH^- species leads to the

generation of $^{\bullet}O_2^-$, OH$^{\bullet}$, and other radical species, which are very effective in decomposing pollutants in water.[53]

3.5. Mechanism for photocatalytic degradation activity

To study the mechanism of photocatalytic degradation assisted by high-quality ZnO NRs, an aqueous docosane solution (10 ppm) was used as a petroleum contaminant under a solar light simulator. Fig. 5(a) illustrates the photocatalytic degradation process of docosane after 5 hours of exposure in the solar irradiation simulator. In addition, the GC-MS/MS technique was utilized to estimate the degradation efficiency mechanism and measure the initial (C_0) and final (C) concentration of the compound using the following formula:[54]

$$\text{Degradation efficiency } (\%) = \left(\frac{C_0 - C}{C_0}\right) \times 100 \qquad (3)$$

Docosane was 68.5% degraded in the presence of the ZnO NR photocatalysts after five hours of exposure to solar simulator light, as determined using GC-MS/MS analysis. In the absence of the ZnO NRs under same conditions, there is no significant change in the concentration of the compound. This implies that the organic contaminant docosane does not break down readily in the absence of ZnO NR photocatalytic supports.[55,56] The effectiveness of photocatalysis in removing organic compounds may vary significantly based on the quantities of the compounds, their age, geological location, and additives used in their extraction.[22,57]

Experiments were further examined at different initial concentrations of docosane (5, 15, 20, and 25 ppm) in a photocatalytic degradation process in the presence of the ZnO NRs at room temperature under identical conditions. GC-MS/MS analysis indicates an increase in the area with concentration, as shown in Fig. 5(b). Similar results have been reported in the literature on the decomposition of harmful organic compounds and effectiveness of the application of the ZnO NRs as a photocatalyst in water treatment.[24,41,58] The analysis of GC-MS/MS results on the effectiveness of the photocatalytic degradation of the ZnO NRs of docosane at 5 hours is shown in Fig. 5(c). Through analysis of the results, it appears that docosane exhibits an intense peak at a retention time of 16.62 minutes at the beginning of the photocatalysis process, and the peak intensity decreases after a certain period. This reduction is driven by the photocatalytic effectiveness of the ZnO NRs, which oxidize organic chemicals into non-toxic products. When the

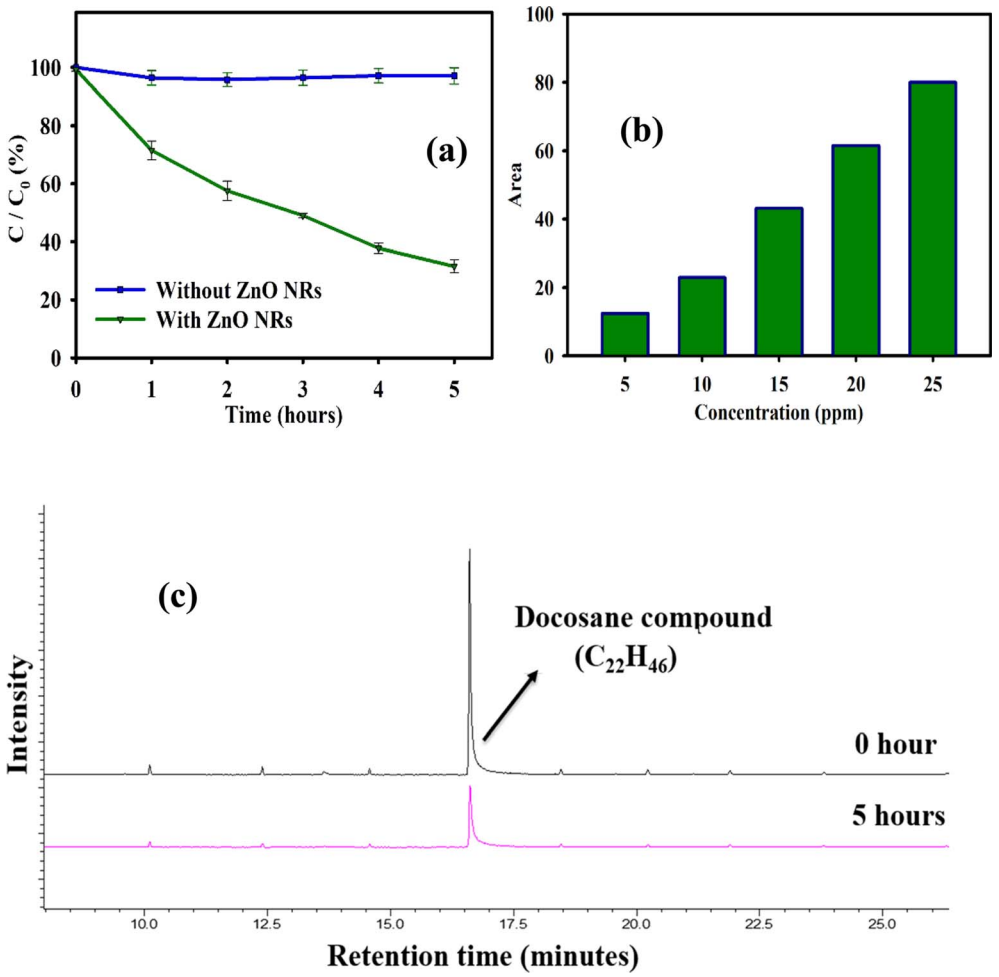

Fig. 5 GC-MS/MS analysis of docosane: (a) concentration at different time intervals, (b) effect of initial concentration (5, 10, 15, 20, and 25 ppm), and (c) peaks at irradiation times of 0 and 5 hours during photocatalysis.

photons collide with the surface of the ZnO NRs, the mechanism of the photocatalysis process in mitigating toxic organic materials is attributed to the rapid recombination of charge carriers, which photoexcites e^-/h^+ pairs in the VB to the CB to react with O_2 and H_2O to produce $^{\bullet}O_2^-$ and $OH^{\bullet}$ radicals.

Thus, the e^-/h^+ pairs trapped in the surface defects of the ZnO NRs generate free radicals that directly catalyze redox interactions with organic materials to degrade contaminated water. The mechanism of the photocatalytic degradation of organic compounds in the presence of ZnO nanorods and their oxidation to H_2O, CO_2, and by-products is characterized by a sequence of chemical equations[59–61] as follows:

$$ZnO + h\nu \rightarrow ZnO\ (e_{CB}^- + h_{VB}^+) \quad (4)$$

$$e_{CB}^- + O_2 \rightarrow {}^{\bullet}O_2^- \quad (5)$$

$$^{\bullet}O_2^- + H_2O \rightarrow {}^{\bullet}HO_2 + OH^- \quad (6)$$

$$h_{VB}^+ + OH^- \rightarrow OH^{\bullet} \quad (7)$$

$$^{\bullet}O_2^- + \text{organic compounds} \rightarrow H_2O + CO_2\ (\text{reduction reaction}) \quad (8)$$

$$OH^{\bullet} + \text{organic compounds} \rightarrow H_2O + CO_2\ (\text{oxidation reaction}) \quad (9)$$

The existence of sufficient e^-/h^+ pairs created *via* the photocatalytic degradation process to form free radicals on the ZnO NR surfaces results in photocatalytic performance that is suitable for the degradation of the docosane molecule, as shown by equations.[4–9]

In the CB, O_2 is easily absorbed on the surface of the ZnO NRs catalyst in a reduction reaction that leads to an electron scavenger (electron acceptor). This causes the formation of types of strong oxidizing radicals that react directly with organic compounds and convert them to H_2O, CO_2, and other safe products. Conversely, the excited hole scavenger (electron donor) in the VB causes an oxidation reaction with H_2O or organic compounds. Therefore, the generated holes help create free radicals by oxidizing H_2O or organic compounds to H_2O, CO_2, and other safe products. In addition, the electrons generated in the semiconductor band act as an electron transfer medium between the VB and CB with an acceptor/donor pair in reduction/oxidation reactions, facilitating the reaction with oxygen and splitting of water and compounds. The reduction and oxidation efficiency of photocatalysts may be affected by an upward shift of the CB and a downward shift of the VB through quantum confinement and intrinsic defects in semiconductors.[62,63] Fig. 6 schematically illustrates a pathway to a charge transfer mechanism and radical generation processes in the ZnO semiconductor domain during the 68.5% photocatalytic degradation of docosane. Ghafoori *et al.* reported that the performance and efficiency of the photocatalytic process could result in the removal of about 90% of the hydrocarbons from OPW. However, the efficiency photocatalysis may vary depending on the environmental and operating parameters of the sample.[57]

To investigate the kinetics of the photocatalytic degradation of a molecule according to the Langmuir–Hinshelwood model, the pseudo-first-order kinetics rate constant (k) was analyzed. The photocatalytic reaction kinetics are represented by observed apparent rate constants (k) and correlation coefficients (R^2) as per the following relation:[64]

$$\ln\left(\frac{C_0}{C}\right) = kt \quad (10)$$

As shown in Fig. 7, the reaction kinetics of the photocatalytic degradation of a docosane molecule supported by the ZnO NRs were determined by plotting $\ln(C_0/C)$ *vs.* time (t). The rate constant of the photocatalytic degradation was found to be $k = 0.2407\ h^{-1}$ with an R^2 value of 0.9805.

The value of $k = 0.2407\ h^{-1}$ indicates that the degradation reaction proceeds at a rate of $0.2407\ h^{-1}$, *i.e.*, about 24.07% of the docosane is degraded every hour during the photocatalytic process experiment. The R^2 value of close to 1 suggests that the pseudo-first-order model used to describe the photocatalytic degradation process accurately represents experimental data. The R^2 value of 0.9805 indicates a very good fit, suggesting that the kinetic model used in this study closely matches the degradation efficiency equation of docosane under given experimental conditions. It can be noted that a higher k value indicates a faster

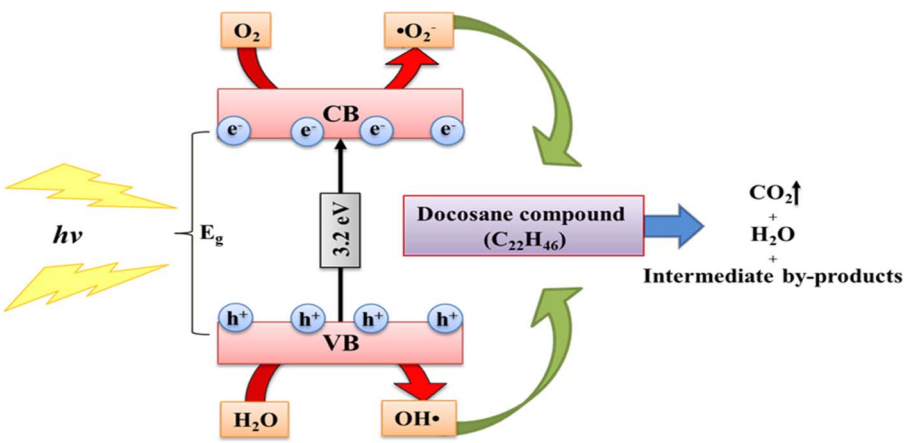

Fig. 6 Schematic model of the degradation mechanism of docosane by the ZnO NR photocatalyst.

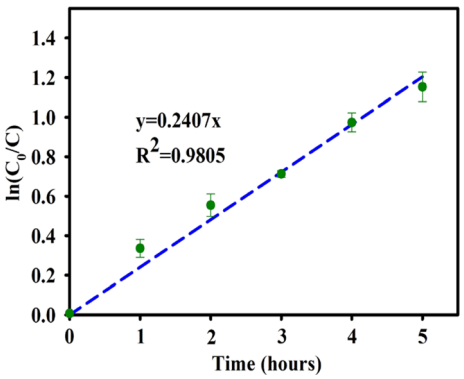

Fig. 7 Pseudo-first-order kinetic plot for the photocatalytic degradation of docosane.

reaction rate, while a higher R^2 value closer to 1 indicates a better fit for the model used in experimental data.[65,66]

The effectiveness of the photocatalytic process was controlled using the pH and the total organic carbon (TOC).[67] Parmar *et al.* indicated that the productivity of photolysis is influenced by the amount of catalyst employed, the pH of the solution, the concentration, and the duration of irradiation.[68] The docosane solution was maintained at a stable pH in the absence of the ZnO NRs during the photocatalysis process. However, in the presence of the ZnO NRs, the photocatalytic degradation of the docosane solution was influenced by the pH value, as shown in Fig. 8(a). The initial pH of 7.71 gradually decreases to ~6.5 at the end of the process.

The chemical reaction of the photocatalytic process and basic structure of ZnO NRs may be affected by changes in the pH of the solution.[69] Abdullah Goktas *et al.* confirmed that the pH of a solution could change the surface charge of the ZnO NRs and dissolution efficiency of the photocatalysis process. Therefore, the high pH contributes to the presence of large amounts of hydroxyl radicals that oxidize organic molecules to safe chemicals along the efficient decomposition pathway.[70]

This property can be explained by the fact that low pH levels cause positive charges to assemble on the surface of the ZnO NRs. This affects the production of free radicals and transfer of these radicals in photocatalytic reaction bands under experimental conditions. Alsharyani *et al.* demonstrated that lower pH values contribute to the efficiency of photocatalytic degradation to affect the surface charge of the catalysts, which is attributed to the production of free radicals, leading to improved degradation of pollutant molecules.[35] During the photocatalytic process, free radicals (like $OH^{\bullet}$ and $^{\bullet}O_2^-$) are generated who react with organic compounds and water molecules. This direct reaction results in the production of protons (H^+) and hydroxide ions (OH^-), which causes an increase in H^+ ions to lower the pH, making the solution pH exhibit an acidic slope.[71] The efficiency of the photocatalytic degradation process decreases and is affected by the rise in pH; the radicals are quickly scavenged and not able to react, causing little adsorption.[34,72] Liang *et al.* reported that if the pH is high, the ZnO NR surface will be negatively charged, which facilitates the transfer of molecules and generates an abundance of ($OH^{\bullet}$) radicals that contribute to affect the photocatalytic degradation process.[73] On the contrary, the change in pH values also occurs due to the presence of organic compounds resulting from transformations in the photocatalytic process. Thus, the photocatalytic degradation persists in the redox process of the organic materials, until it leads to the breakage of compound bonds and formation of unstable intermediate by-products, which eventually transform into H_2O and CO_2. Therefore, the presence of these intermediate by-products in the solution affects the photocatalytic degradation activity.

Fig. 8(b) shows the percent TOC removed at various time intervals during the photocatalytic degradation of the organic pollutant docosane under optimal testing conditions. In the presence of the ZnO nanorods, the photocatalytic process was able to remove 60.5% more total organic carbon (TOC) than in the absence of the ZnO NRs. The degradation rate initially increases gradually until 5 hours of exposure, after which it remains constant. The degree of organic material degradation is proportional to the proven efficiency of the photocatalysis process, as shown by the removal of total organic carbon (TOC).[74] The fact of limited and ambient amount of experimental work in the photocatalysis process makes the production of intermediate by-products inevitable. However, this does not indicate the efficiency of the photocatalysis process; rather, it signifies its ability to convert organic contaminants into chemicals that are harmless to the environment.

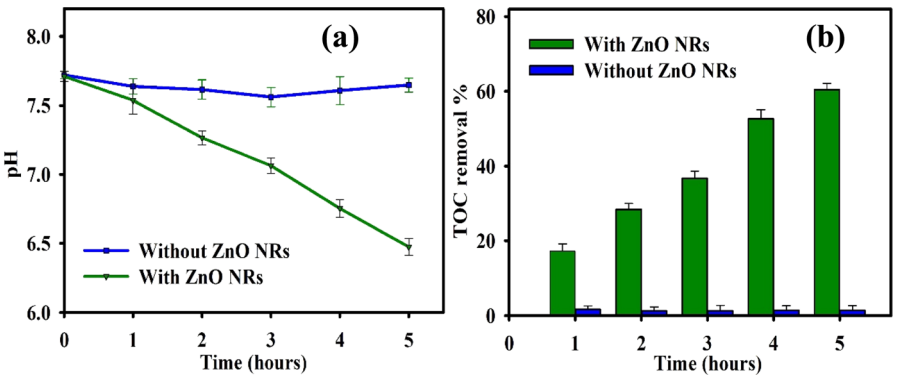

Fig. 8 Effect of parameters on the photocatalytic degradation of docosane: (a) pH value and (b) TOC analysis.

4. Conclusions

Photocatalytic activity supported by the ZnO NRs was investigated to remediate docosane, an organic pollutant compound present in OPW, under a solar light simulator. The ZnO NRs were efficiently synthesized using a microwave-assisted hydrothermal method on the glass substrates. The morphological and hexagonal Wurtzite properties of the ZnO NRs were analyzed using SEM and XRD. Evaluation of EDS data reveals the absence of impurities or foreign elements in the basic composition of ZnO NRs. Using UV-Vis and PL devices, the optical characteristics of pure ZnO NRs were obtained and indicated an E_g value of 3.20 eV and surface defect states, respectively. A 10 ppm solution of the organic contaminant docosane was prepared to study the mechanism of the photocatalytic process. When exposed to radiation, the surface area of the ZnO NRs absorbs photons, triggering the excitation of the e^-/h^+ pairs between the VB and CB in the photocatalysis process to form free radicals that react directly with organic contaminants and convert them into benign chemicals. Further, 68.5% of docosane molecules were degraded with a rate constant of 0.2407 h^{-1}, demonstrating the effectiveness of the ZnO-NR-assisted photocatalysis process as confirmed by GC-MS/MS analytical data. In addition, around 60.5% of the total organic carbon was removed, resulting in a pH of about 6.5. This research on the degradation of the compound docosane is the first using a photocatalytic process, from which intermediate by-products can be identified and studied in the future. These findings constitute a successful example of a photocatalytic degradation process for organic molecules in OPW, as well as a hopeful and bright beginning point for the safe development of the environment.

Conflicts of interest

The authors declare that they have no known competing financial interests or personal relationships that could have appeared to influence the work reported in this paper.

Acknowledgements

The authors are truly grateful to the Central Analytical and Applied Research Unit (CAARU) at Sultan Qaboos University and the Nanotechnology Research Center in the Department of Petroleum and Chemical Engineering. They extend special thanks to Dr Mohammad Al-Abri, Dr Jamal Al-Sabahi, and Dr Issa Al-Hussaini at Sultan Qaboos University for the discussion and technical assistance throughout trials. The authors would also like to thank the Muscat Municipality for their assistance with GC-MS/MS.

References

1 S. Nadersha and A. Aly Hassan, Biodesalination and treatment of raw hypersaline produced water samples using indigenous wastewater algal consortia, *Desalination*, 2022, **528**, 115638.
2 E. T. Igunnu and G. Z. Chen, Produced water treatment technologies, *Int. J. Low-Carbon Technol.*, 2012, **9**(3), 157–177.
3 A. Olajire Abass, Recent advances on the treatment technology of oil and gas produced water for sustainable energy industry-mechanistic aspects and process chemistry perspectives, *Chem. Eng. J. Adv.*, 2020, **4**, 100049.
4 M. Al-Salmi, M. Laqbaqbi, S. Al-Obaidani, R. S. Al-Maamari, M. Khayet and M. Al-Abri, Application of membrane distillation for the treatment of oil field produced water, *Desalination*, 2020, **494**, 114678.
5 L. T. Popoola, A. S. Yusuff, A. A. Adeyi and O. O. Omotara, Adsorptive removal of heavy metals from oil well produced water using citrullus lanatus peel: characterization and optimization, *S. Afr. J. Chem. Eng.*, 2022, **39**, 19–27.
6 Z. Chen, L. Zhao, K. Lee and C. Hannath, Modeling and Assessment of the Produced Water Discharges from Offshore Petroleum Platforms, *Water Qual. Res. J.*, 2007, **42**(4), 303–310.
7 L. Manfra, G. Moltedo, C. V. Lamberti, C. Maggi, M. G. Finoia, S. Giuliani, *et al.*, Metal Content and Toxicity of Produced Formation Water (PFW): Study of the Possible Effects of the Discharge on Marine Environment, *Arch. Environ. Contam. Toxicol.*, 2007, **53**(2), 183–190.
8 Y. Liu, Y. Li, H. Lu, Z. Pan, P. Dai, G. Sun, *et al.*, A full-scale process for produced water treatment on offshore oilfield: reduction of organic pollutants dominated by hydrocarbons, *J. Cleaner Prod.*, 2021, **296**, 126511.
9 C. Yang, W. Kuang, G. Zhang, S. Mortazavi, A. Doiron, K. Volchek, *et al.*, Characterization of residual organic matter in oil sands steam assisted gravity drainage produced water treated by ceramic nanofiltration membranes, *J. Pet. Sci. Eng.*, 2022, **208**, 109408.
10 J. Neff, T. C. Sauer and A. D. Hart, Bioaccumulation of Hydrocarbons from Produced Water Discharged to Offshore Waters of the US Gulf of Mexico, *Produced Water*, 2011, 441–477.
11 B. Rajasekhar, I. M. Nambi and S. K. Govindarajan, Investigating the degradation of nC_{12} to nC_{23} alkanes and PAHs in petroleum-contaminated water by electrochemical advanced oxidation process using an inexpensive Ti/Sb-SnO_2/PbO_2 anode, *Chem. Eng. J.*, 2021, **404**, 125268.
12 F. Mao, J. Wang and H. Fan, Application of two-dimensional gas chromatography/time-of-flight mass spectrometry (GC × GC-TOFMS) for the thorough study of hydrocarbons in lignite pyrolysates, *J. Anal. Appl. Pyrolysis*, 2021, **157**, 105178.
13 A. Ravi, M. Ravuri, R. Krishnan, J. Narenkumar, K. Anu, M. S. Alsalhi, *et al.*, Characterization of petroleum degrading bacteria and its optimization conditions on effective utilization of petroleum hydrocarbons, *Microbiol. Res.*, 2022, **265**, 127184.
14 M. Goswami, R. Patowary, K. Patowary, H. P. Sarma, S. Rabha, B. Devi, *et al.*, Environment friendly treatment of petroleum hydrocarbon contaminated formation water: mechanisms and consequences for degradation and adsorption, *Water Resour. Ind.*, 2023, **30**, 100224.
15 L.-G. Faksness, P. G. Grini and P. S. Daling, Partitioning of semi-soluble organic compounds between the water phase

and oil droplets in produced water, *Mar. Pollut. Bull.*, 2004, **48**(7–8), 731–742.
16 K. Hylland, Polycyclic Aromatic Hydrocarbon (PAH) Ecotoxicology in Marine Ecosystems, *J. Toxicol. Environ. Health, Part A*, 2006, **69**(1–2), 109–123.
17 J. Tang, M. Wang, F. Wang, Q. Sun and Q. Zhou, Eco-toxicity of petroleum hydrocarbon contaminated soil, *J. Environ. Sci.*, 2011, **23**(5), 845–851.
18 J. M. Neff and R. Hagemann, Environmental Challenges of Heavy Crude Oils: Management of Liquid Wastes, *E&P Environmental and Safety Conference*, Texas, U.S.A., 2007.
19 M. K. Purkait, A. Maiti, S. DasGupta and S. De, Removal of congo red using activated carbon and its regeneration, *J. Hazard. Mater.*, 2007, **145**(1–2), 287–295.
20 A. Z. Rodriguez, H. Wang, L. Hu, Y. Zhang and P. Xu, Treatment of Produced Water in the Permian Basin for Hydraulic Fracturing: Comparison of Different Coagulation Processes and Innovative Filter Media, *Water*, 2020, **12**(3), 770.
21 M. T. Binet, J. L. Stauber and T. Winton, The Effect of Storage Conditions on Produced Water Chemistry and Toxicity, *Produced Water*, 2011, 163–179.
22 S. Jiménez, M. M. Micó, M. Arnaldos, F. Medina and S. Contreras, State of the art of produced water treatment, *Chemosphere*, 2018, **192**, 186–208.
23 S. O. Ganiyu, S. Sable and M. Gamal El-Din, Advanced oxidation processes for the degradation of dissolved organics in produced water: a review of process performance, degradation kinetics and pathway, *Chem. Eng. J.*, 2022, **429**, 132492.
24 J. Al-Sabahi, T. Bora, M. Claereboudt, M. Al-Abri and J. Dutta, Visible light photocatalytic degradation of HPAM polymer in oil produced water using supported zinc oxide nanorods, *Chem. Eng. J.*, 2018, **351**, 56–64.
25 G. P. Anipsitakis and D. D. Dionysiou, Degradation of Organic Contaminants in Water with Sulfate Radicals Generated by the Conjunction of Peroxymonosulfate with Cobalt, *Environ. Sci. Technol.*, 2003, **37**(20), 4790–4797.
26 Z. Oksida-Polivinilpirolidon, Photocatalytic degradation of industrial dye wastewater using zinc oxide-polyvinylpyrrolidone nanoparticles, *Malaysian Journal of Analytical Science*, 2018, **22**(4), 693–695.
27 H. J. Biswal, T. Srivastava, P. R. Vundavilli and A. Gupta, Facile fabrication of hydrophobic ZnO nanostructured nickel microtubes through pulse electrodeposition as promising photocatalyst for wastewater remediation, *Journal of Manufacturing Processes*, 2022, **75**, 538–551.
28 O. Seven, B. Dindar, S. Aydemir, D. Metin, M. A. Ozinel and S. Icli, Solar photocatalytic disinfection of a group of bacteria and fungi aqueous suspensions with TiO_2, ZnO and Sahara desert dust, *J. Photochem. Photobiol., A*, 2004, **165**(1–3), 103–107.
29 J. S. Chang, Y. W. Phuan, M. N. Chong and J. D. Ocon, Exploration of a novel Type II 1D-ZnO nanorods/$BiVO_4$ heterojunction photocatalyst for water depollution, *J. Ind. Eng. Chem.*, 2020, **83**, 303–314.
30 A. Ullah, M. Saadullah, F. Alvi, L. Sherin, A. Ali, N. A. Shad, *et al.*, Synergistic effect of silver doped ZnO nanomaterials enhances the anticancer potential against A459 lung cancer cells, *J. King Saud Univ., Sci.*, 2022, **34**(1), 101724.
31 S. Baruah, M. A. Mahmood, M. T. Myint, T. Bora and J. Dutta, Enhanced visible light photocatalysis through fast crystallization of zinc oxide nanorods, *Beilstein J. Nanotechnol.*, 2010, **1**, 14–20.
32 M. Sanjeeva Gandhi and Y. S. Mok, Shape-dependent plasma-catalytic activity of ZnO nanomaterials coated on porous ceramic membrane for oxidation of butane, *Chemosphere*, 2014, **117**, 440–446.
33 J. Al-Sabahi, T. Bora, M. Al-Abri and J. Dutta, Efficient visible light photocatalysis of benzene, toluene, ethylbenzene and xylene (BTEX) in aqueous solutions using supported zinc oxide nanorods, *PLoS One*, 2017, **12**(12), e0189276.
34 H. Al-Hasani, J. Al-Sabahi, B. Al-Ghafri, R. Al-Hajri and M. Al-Abri, Effect of water quality in photocatalytic degradation of phenol using zinc oxide nanorods under visible light irradiation, *J. Water Process Eng.*, 2022, **49**, 103121.
35 A. K. Alsharyani and L. Muruganandam, Photocatalytic degradation of eicosane and phytane compounds using support zinc oxide nanorods under solar simulator irradiation, *J. Water Process Eng.*, 2023, **53**, 103837.
36 B. Al Farsi, F. Al Marzouqi, M. Al-Maashani, M. T. Souier, M. Tay Zar Myint and M. Z. Al-Abri, Rapid microwave-assisted fabrication of Al-doped zinc oxide nanorods on a glass substrate for photocatalytic degradation of phenol under visible light irradiation, *Mater. Sci. Eng., B*, 2021, **264**, 114977.
37 V. Yadav, N. Singh and D. Meena, Investigation of structural and optical properties of pure SnO_2, ZnO and SnO_2/ZnO composite nanorods, *Mater. Today: Proc.*, 2022, **62**, 3368–3375.
38 Z. Chamanzadeh, V. Ansari and M. Zahedifar, Investigation on the properties of La-doped and Dy-doped ZnO nanorods and their enhanced photovoltaic performance of Dye-Sensitized Solar Cells, *Opt. Mater.*, 2021, **112**, 110735.
39 S. S. A. Al Ghafry, M. Z. Al-Abri, B. Al Farsi, F. Al Marzouqi, L. M. Al Farsi, N. A. Roslan, *et al.*, Ga-doped ZnO nanorods: the photocatalytic performance of methylene blue under solar irradiation, *Opt. Mater.*, 2022, **126**, 112139.
40 A. A. Mohd Raub, J. Yunas, M. A. Mohamed, B. Bais, A. A. Hamzah, J. Ridwan, *et al.*, Synthesis and characterization of ZnO NRs with spray coated GO for enhanced photocatalytic activity, *Ceram. Int.*, 2022, **48**(13), 18238–18245.
41 A. El Golli, M. Fendrich, N. Bazzanella, C. Dridi, A. Miotello and M. Orlandi, Wastewater remediation with ZnO photocatalysts: green synthesis and solar concentration as an economically and environmentally viable route to application, *J. Environ. Manage.*, 2021, **286**, 112226.
42 M. Nami, A. Rakhsha, S. Sheibani and H. Abdizadeh, The enhanced photocatalytic activity of ZnO nanorods/CuO nanourchins composite prepared by chemical bath precipitation, *Mater. Sci. Eng., B*, 2021, **271**, 115262.

43 A. F. Abdulrahman, N. M. Abd-Alghafour and M. A. Almessiere, A high responsivity, fast response time of ZnO nanorods UV photodetector with annealing time process, *Opt. Mater.*, 2023, **141**, 113869.

44 S. Kaya, O. Ozturk and L. Arda, Vertically aligned Nd substituted ZnO nanorods: morphology, optical characteristics and room temperature ferromagnetism, *Curr. Appl. Phys.*, 2022, **35**, 45–57.

45 N. Patra, M. Manikandan, V. Singh and I. A. Palani, Investigations on LSPR effect of Cu/Al nanostructures on ZnO nanorods towards photodetector applications, *J. Lumin.*, 2021, **238**, 118331.

46 G. H. Mhlongo, K. Shingange, Z. P. Tshabalala, B. P. Dhonge, F. A. Mahmoud, B. W. Mwakikunga, *et al.*, Room temperature ferromagnetism and gas sensing in ZnO nanostructures: influence of intrinsic defects and Mn, Co, Cu doping, *Appl. Surf. Sci.*, 2016, **390**, 804–815.

47 N. F. Nazari, M. Rajabi and A. Z. Moshfegh, The UV photodetection enhancement of tailored ZnO nanorods by controlling the aspect ratio, *Surf. Interfaces*, 2022, **28**, 101682.

48 F. Shahzad, A. Qamar and G. Nabi, Significant enhancement in field emission and photoluminescence properties of vertically aligned tellurium nanorods by plasma treatment, *Opt. Mater.*, 2022, **126**, 112171.

49 Y. He, Y. Wang, Y. Guo and L. Ma, Fine adjustment of emission wavelength, light-conversion quality, photostability of blue-violet light conversion agents based on FRET effect, *Dyes Pigm.*, 2023, **217**, 111429.

50 V. Khomchenko, M. Sopinskyy, M. Mazin, V. Dan'ko, O. Lytvyn and Y. Piryatinskii, The violet luminescence band in ZnO and ZnO-Ag thin films, *J. Lumin.*, 2019, **213**, 519–524.

51 I. Boukhoubza, M. Khenfouch, M. Achehboune, B. M. Mothudi, I. Zorkani and A. Jorio, Graphene oxide/ZnO nanorods/graphene oxide sandwich structure: the origins and mechanisms of photoluminescence, *J. Alloys Compd.*, 2019, **797**, 1320–1326.

52 P. Molaei and F. Rahimi Moghadam, Seed-free synthesis of ZnO nanorods through egg white/glycerol medium for photocatalyst applications, *Mater. Today Commun.*, 2022, **31**, 103677.

53 T. Bora, P. Sathe, K. Laxman, S. Dobretsov and J. Dutta, Defect engineered visible light active ZnO nanorods for photocatalytic treatment of water, *Catal. Today*, 2017, **284**, 11–18.

54 D. Akyüz, rGO-TiO_2-CdO-ZnO-Ag photocatalyst for enhancing photocatalytic degradation of methylene blue, *Opt. Mater.*, 2021, **116**, 111090.

55 M. A. Al-Gharibi, H. H. Kyaw, J. N. Al-Sabahi, M. T. Zar Myint, Z. A. Al-Sharji and M. Z. Al-Abri, Silver nanoparticles decorated zinc oxide nanorods supported catalyst for photocatalytic degradation of paracetamol, *Mater. Sci. Semicond. Process.*, 2021, **134**, 105994.

56 C. Belabed, A. Tab, F. Moulai, O. Černohorský, S. Boudiaf, N. Benrekaa, *et al.*, ZnO nanorods-PANI heterojunction dielectric, electrochemical properties, and photodegradation study of organic pollutant under solar light, *Int. J. Hydrogen Energy*, 2021, **46**(40), 20893–20904.

57 S. Ghafoori, M. Omar, N. Koutahzadeh, S. Zendehboudi, R. N. Malhas, M. Mohamed, *et al.*, New advancements, challenges, and future needs on treatment of oilfield produced water: a state-of-the-art review, *Sep. Purif. Technol.*, 2022, **289**, 120652.

58 G. Mahmodi, A. Ronte, S. Dangwal, P. Wagle, E. Echeverria, B. Sengupta, *et al.*, Improving antifouling property of alumina microfiltration membranes by using atomic layer deposition technique for produced water treatment, *Desalination*, 2022, **523**, 115400.

59 B. Baruah, L. Downer and D. Agyeman, Fabric-based composite materials containing ZnO-NRs and ZnO-NRs-AuNPs and their application in photocatalysis, *Mater. Chem. Phys.*, 2019, **231**, 252–259.

60 A. Somdee and S. Wannapop, Enhanced photocatalytic behavior of ZnO nanorods decorated with a Au, $ZnWO_4$, and Au/ZnWO4 composite: synthesis and characterization, *Colloid Interface Sci. Commun.*, 2022, **47**, 100591.

61 L. P. P. Ha, T. H. T. Vinh, N. T. B. Thuy, C. M. Thi and P. V. Viet, Visible-light-driven photocatalysis of anisotropic silver nanoparticles decorated on ZnO nanorods: synthesis and characterizations, *J. Environ. Chem. Eng.*, 2021, **9**(2), 105103.

62 W. David Wei, J. S. DuChene, B. C. Sweeny, J. Wang and W. Niu, Chapter 12 - Current Development of Photocatalysts for Solar Energy Conversion, in *New and Future Developments in Catalysis*, ed. S. L. Suib, Elsevier, Amsterdam, 2013, pp. 279–304.

63 D. Kong, Y. Zheng, M. Kobielusz, Y. Wang, Z. Bai, W. Macyk, *et al.*, Recent advances in visible light-driven water oxidation and reduction in suspension systems, *Mater. Today*, 2018, **21**(8), 897–924.

64 N. L. Gavade, A. N. Kadam, S. B. Babar, A. D. Gophane, K. M. Garadkar and S.-W. Lee, Biogenic synthesis of gold-anchored ZnO nanorods as photocatalyst for sunlight-induced degradation of dye effluent and its toxicity assessment, *Ceram. Int.*, 2020, **46**(8), 11317–11327.

65 R. K. Das, D. Pal and U. Sarkar, Efficacy of convective-diffusion models to study the transient behaviour of a sewage-sludge-filled packed column for aqueous phase adsorption of fluoroquinolones: consideration of pseudo-kinetics driven depletion of species, *J. Environ. Chem. Eng.*, 2023, **11**(3), 109896.

66 M. H. Mahmoudian, A. Azari, A. Jahantigh, M. Sarkhosh, M. Yousefi, S. A. Razavinasab, *et al.*, Statistical modeling and optimization of dexamethasone adsorption from aqueous solution by Fe_3O_4@NH_2-MIL88B nanorods: isotherm, kinetics, and thermodynamic, *Environ. Res.*, 2023, **236**, 116773.

67 Y. Qin, B. Yang, H. Li and J. Ma, Immobilized $BiOCl_{0.75}I_{0.25}$/g-C_3N_4 nanocomposites for photocatalytic degradation of bisphenol A in the presence of effluent organic matter, *Sci. Total Environ.*, 2022, **842**, 156828.

68 N. Parmar and J. K. Srivastava, Process optimization and kinetics study for photocatalytic ciprofloxacin degradation

using TiO_2 nanoparticle: a comparative study of Artificial Neural Network and Surface Response Methodology, *J. Indian Chem. Soc.*, 2022, **99**(8), 100584.

69 W. Gao, Y. Liu and J. Dong, Immobilized ZnO based nanostructures and their environmental applications, *Prog. Nat. Sci.: Mater. Int.*, 2021, **31**(6), 821–834.

70 A. Goktas, E. Aslan, F. Arslan and A. Kilic, Characterization of multifunctional solution-processed $Sn_{1-x}Zn_xS$ nanostructured thin films for photosensitivity and photocatalytic applications, *Opt. Mater.*, 2022, **133**, 112984.

71 X. Li, H. Song, G. Zhang, W. Zou, Z. Cao, Y. Pan, *et al.*, Enhanced organic pollutant removal in saline wastewater by a tripolyphosphate-Fe^0/H_2O_2 system: key role of tripolyphosphate and reactive oxygen species generation, *J. Hazard. Mater.*, 2023, **457**, 131821.

72 A. F. Alkaim, A. M. Aljeboree, N. A. Alrazaq, S. J. Baqir, F. H. Hussein and A. J. Lilo, Effect of pH on Adsorption and Photocatalytic Degradation Efficiency of Different Catalysts on Removal of Methylene Blue, *Asian J. Chem.*, 2014, **26**(24), 8445–8448.

73 F. Liang, Y.-H. Zhang, B. He, J. Yang, Q. Shi and F.-N. Shi, Enhanced photocatalytic degradation of imidacloprid and RhB by the precursor derived $Bi_{12.7}Co_{0.3}O_{19.35}$ under different pH value, *J. Phys. Chem. Solids*, 2022, **164**, 110638.

74 E. S. Behineh, A. R. Solaimany Nazar, M. Farhadian and M. Moghadam, Photocatalytic degradation of cefixime using visible light-driven Z-scheme ZnO nanorod/Zn_2TiO_4/GO heterostructure, *J. Environ. Manage.*, 2022, **316**, 115195.